Stretch-driven microfluidic chip for nucleic acid detection

Xiang Li[a], Xiaoyu Zhao[a], Weihao Yang[a], Fei Xu[a], Bailiang Chen[a], Jiwei Peng[a], Jiajun Huang[a b*], Shengli Mi[a*]

a. Bio-manufacturing Engineering Laboratory, Tsinghua Shenzhen International Graduate School, Tsinghua University, Shenzhen, Guangdong 518000, China.

b. Optometry Advanced Medical Equipment R&D Center, Research Institute of Tsinghua University in Shenzhen, Nanshan District, Shenzhen, Guangdong, 518000, China.Tel: +86-17707560361;E-mail: vt_bongo@hotmail.com.

***Corresponding author:**

Shengli Mi

Tsinghua Shenzhen International Graduate School, Tsinghua University,

Rm 1110, Energy and environment Building, Tsinghua Campus,

The University Town, Shenzhen 518055, P. R. China

Tel: +86 (0)755 26036329;

Fax: +86(0)755 26036356;

E-mail: mi.shengli@sz.tsinghua.edu.cn

Jiajun Huang

Tsinghua Shenzhen International Graduate School, Tsinghua University,

Rm 1104, Energy and environment Building, Tsinghua Campus,

The University Town, Shenzhen 518055, P. R. China

Optometry Advanced Medical Equipment R&D Center, Research Institute of Tsinghua University in Shenzhen, Nanshan District, Shenzhen, Guangdong, 518000, China

Tel: +86-17707560361;

E-mail: vt_bongo@hotmail.com

Abstract

Molecular diagnosis is an essential means to detect pathogens. The portable nucleic acid detection chip has excellent prospects in places where medical resources are scarce, and it is also of research interest in the field of microfluidic chips. Here, the paper developed a new type of microfluidic chip for nucleic acid detection where stretching acts as the driving force. The sample entered the chip by applying capillary force. The strain valve was opened under the action of tensile force, and the spring pump generated the power to drive the fluid to flow to the detection chamber in a specific direction. The detection of COVID-19 was realized on the chip. The RT-LAMP amplification system was adopted to observe the liquid color in the detection chamber to decide whether the sample tested positive or negative qualitatively.

Keywords

Microfluidics, Nucleic acid detection, Stretch-driven, Hand-powered

1. Introduction

Many major diseases have been caused by viruses and prone to global security emergencies(Koonin, 2020). A molecular diagnosis is an effective tool for disease screening. Usually, nucleic acids concentrations of the obtained samples, such as blood or urine, are low and requires amplification as a means to achieve detection. Nucleic acid detection is an effective and practical means for disease screening. However, traditional detection methods like polymerase chain reaction (PCR) and single nucleotide polymorphism (SNP) require people who are experienced in handling multiple reagents and need bulky equipment, which is inaccessible to efficient and low-cost detections. Many isothermal amplification methods have been developed, including nucleic acid sequence-based amplification (NASBA)(Compton, 1991), recombinase polymerase amplification (RPA)(Schuler et al., 2015), helicase-dependent amplification (HDA)(Vincent, Xu, & Kong, 2004), and loop-mediated isothermal amplification (LAMP)(Z. Yu et al., 2020), which was a new constant temperature nucleic acid amplification method developed by Japanese scholars Notomi et al. in 2000(Notomi et al., 2000). A Bst DNA polymerase was used with strand displacement function, and 4 or 6 primers were specially designed according to 6 regions of the target fragment so that DNA can be amplified at a constant temperature of about 65 ℃. Among these methods, LAMP, in particular, has been widely used in many fields under higher stability, sensitivity, and specificity, especially in real-time diagnosis. In terms of obtaining nucleic acid amplification results, the traditional methods are real-time fluorescence detection and gel electrophoresis, which rely on experimental equipment, making them unsuitable for on-site diagnosis. In recent years, a large number of methods based on direct visual recognition have been developed, such as phosphate colorimetry

and precipitation based on magnesium pyrophosphate. However, these methods are also complex to see the precipitation under ideal conditions (Mori, Kitao, Tomita, & Notomi, 2004; Mori, Nagamine, Tomita, & Notomi, 2001; F. Zhang et al., 2009). Continuous improvement methods for reading the results of LAMP amplification include the use of pH-sensitive dyes(Tanner, Zhang, & Evans, 2015). It is suitable for reading the results directly through vision and being combined in the scene of rapid diagnosis.

As a research tool, microfluidic plays a vital role in biochemical analysis (H. Lee, Park, Ryu, & Jeon, 2014; Li et al., 2014; Temmerman, Huys, & Swings, 2004), which can be used for subsequent clinical diagnosis, nucleic acid detection, and protein analysis. Various microfluidic devices (Nguyen et al., 2019; Song et al., 2021; Syedmoradi, Norton, & Omidfar, 2021) have been developed for other point-of-care testing (POCT). Seung et al. proposed a centrifugal integrated microfluidic chip for detecting a variety of foodborne bacteria by color LAMP (Oh & Seo, 2019). Xin et al. developed a fully integrated nucleic acid detection system to achieve nucleic acid purification, separation, amplification, and detection by real-time fluorescence monitoring(Ye, Li, Wang, Fang, & Kong, 2021). Liu et al. presented a portable food source bacteria detection instrument to achieve sample input and result output(Liu et al., 2020). Although the above devices have reduced the complexity of detection by changing the detection equipment from tube to chip and automating the detection procedure, current methods are still not applicable to a wide range of residents because they (Ji et al., 2020; Strohmeier et al., 2014; B. Yang et al., 2020) require instruments as centrifuges to drive the fluid flow. Therefore, rapid, simple, maneuverable, and efficient nucleic acid detection methods are of significant potential and importance to be developed.

With the improvement of people's living standards, the number of no-external-source microfluidic devices used to monitor human health has gradually increased. They are used to measure heart rate, blood pressure, sweat loss, and other real-time indicators (Gong et al., 2014; Kang, 2019; H. B. Lee, Meeseepong, Trung, Kim, & Lee, 2020; Reeder et al., 2019; N. Yu et al., 2020; Y. Zhang et al., 2020; Z. Zhang, Pi, & Liu, 2015). In addition, some integrated biosensors implement the detection of physiological indicators such as glucose, lactic acid, pH, and cortisol of the organism on the microfluidic chip (Bandodkar et al., 2015; Koh et al., 2016; Sempionatto et al., 2019; X. Yang et al., 2020; Zhong Zhang et al., 2019). The obtained measurement results can be transmitted to the user terminal through wireless equipment to monitor various physiological indicators and physiological state parameters of his/her body in real-time. However, no exogenous microfluidic device is currently used for nucleic acid amplification, which is convenient for personalized users.

In the article, we developed a simple, unpowered microfluidic chip for real-time detection of COVID-19 by colorimetry. A strain valve based on a deformation switch was designed in the chip design process, and its burst pressure was measured. What’s more, the aspect ratio of the spring valve was optimized. In addition, the nucleic acid amplification reaction is realized on both the test tube and the chip, and the GRB values were extracted to represent the color. The normalized value K was used to illustrate the test results, namely positive or negative, of the testing sample.

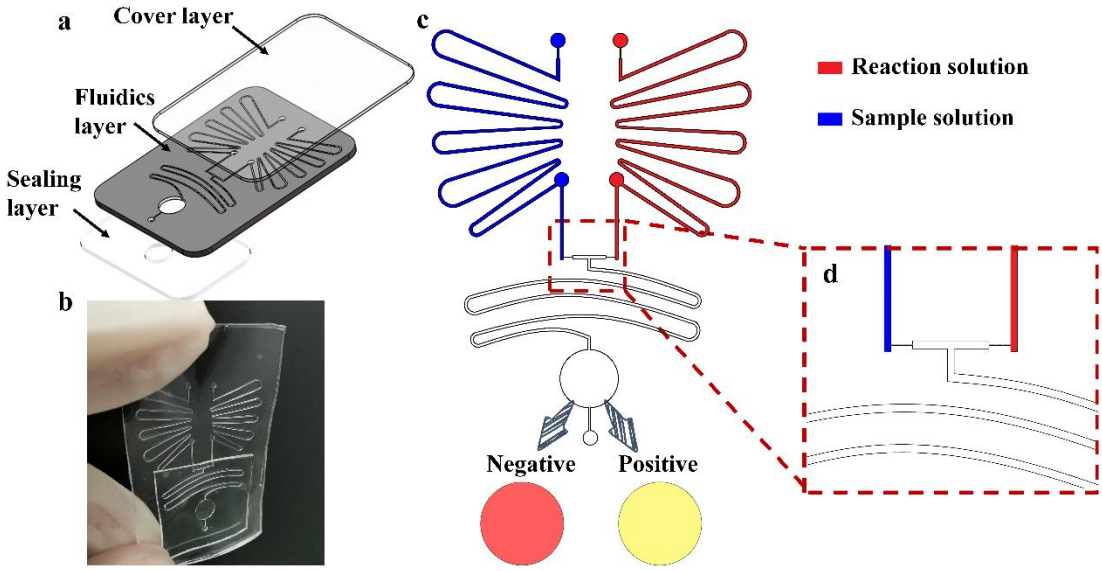

Fig 1 Stretch chip structure. **a** Detailed three-layer structure of the chip. **b** Physical image of the chip. **c** Schematic diagram of the specific design of the runner layer. **d** Magnified view of strain valve and spring pump.

2. Materials and methods

2.1 Materials and reagents

Polydimethylsiloxane (PDMS) and curing agent were obtained from Dow Corning (Ellesworth, cat. no. 184 SIL ELAST KIT 0.5KG). Colorimetric LAMP 2X Master Mix (DNA & RNA) was received from New England Biolabs (Ipswich, MA, USA). 2019-nCoV-N plasmid was synthesized from Guangzhou IGE Biotechnology LTD(Guangzhou, China). Primes were synthesized from shendajiyin (Shenzhen, China), and their sequences are shown in supplementary materials Table S2.

2.2 2019-nCoV-N DNA preparation

For 2019-nCoV-N plasmid synthesis, a standard transformation protocol was used. PCDH-MCS was used as a cloning vector, the insertion site of EcoRI (5') and BamHI (3'). The length

of the cloned sequence was 5369 bp. The details of the cloud sequence are shown in the supplementary material Table S1.

2.3 Device fabrication

The chip was made by three PDMS layers, including a cover layer, a fluidic channel layer, and a sealing layer. The mold for the PDMS layers was fabricated by photolithography. Subsequently, SU-8 2100 was spin-coated to get a 400 μm thickness. In the first step, the photoresist was spin-coated and then exposed to ultraviolet light to obtain the 200 um thickness of the first layer. Next, the mask was aligned with the first layer structure through the microscope alignment cross, and the subsequent ultraviolet light exposure was performed to obtain the second layer structure. The fluidic layer was obtained by mixing PDMS precursors and a curing agent in a ratio of 20:1 and curing it at 80 ℃ for 2 h. After that, the liquid storage chamber formed a through-hole with a diameter of 4.0 mm. The cover layer was obtained by spin-coating a mixture of PDMS and a curing agent with a ratio of 20:1 onto a bare silicon wafer and was cured at 150 ℃ for 5min. Then, a flat needle (19G) was used to punch holes at the entrance. The sealing layer was machined with a PMMA mold. Subsequently, PDMS was baked at 80 ℃ for 2h. Three layers were treated with oxygen plasma for 120 seconds and incubated at 65 ℃ for 10min to seal the chip.

2.4 Elastic modulus measurement

Four groups of PDMS with different ratios were made, which varied from 10:1, 15:1, 20:1 to 25:1. The experimental device was an automatic tensile machine (type of tensile machine). The PDMS specimen was placed on the tensile machine vertically, and the two ends were clamped by pressing the air pump. The curve was obtained by measuring the burden of the test piece

while increasing the displacement. The strain was computed by dividing tensile force with cross-section, while the stress was computed by displacement and length. Consequently, the modulus could be calculated using strain and stress.

2.5 PDMS modified contact angle measurement

Both plasma cleaning and PVP solution coating could realize the hydrophilic modification of PDMS. Five sets of experiments were designed to compare the effects of the above two modification methods. The first group was smooth PDMS. The second group was PDMS coated with PVP solution. The third group was PDMS after plasma cleaning treatment. The fourth group was PDMS that was plasma treated first and then coated with PVP solution. The fifth group was PDMS coated with PVP solution and then plasma treated. Five μl of PVP solution (20%, Ron's reagent, Shanghai) was pipetted on the PDMS surface for 10 minutes and rinsed the surface with water. Water droplets were dropped on the surface of five groups of PDMS, and their modified contacts and their contact angles were measured six days later to observe the timeliness of hydrophilic modification. In addition, the same method was used to measure the contact angles of five different types of liquids, including sweat, saliva, plasma, medium, and ethanol, on the hydrophilic modified PDMS surface.

2.6 Bursting pressure measurement of strain valve

To prove the stain valve could be switched on by stretch-driven, bursting pressure should be measured. The Syringe pump (Chemyx, America) provided continuous and stable displacement, which generated a continuously rising air pressure source through a 5mL needle tube. The Y-shaped three-way connecting pipe (Jiawei Medical Enterprise, Shenzhen, China) led the air pressure evenly generated by the air pressure source to the two channels. One path was to the

chip. The other was to the air pressure sensor (RSCM17100KN030, Dahua Electronic Technology, Shenzhen, China), conducted through the silicone tube (Xinrong Rubber Technology, Shanghai, China). The air pressure sensor was controlled by Arduino (UNO R3, Open Jumper, Chengdu, China) to generate a real-time air pressure curve on the PC side. When the curve dropped, the bursting pressure was read, and this process was repeated three times. In addition, the stretching of the chip was obtained by using a screw slider(G1610, Fuyu Technology, Chengdu, China) controlled by a stepper motor(FM5756SFD04, Fuyu Technology, Chengdu, China).

2.7 Optimized aspect ratio of spring pump

In the chip design, the serpentine flow channel formed a spring pump, whose volume would change through deformation, which could exert pressure to control microfluidics. Five different ratios were designed in Table 1. The corresponding five different types of chips were all made by photolithography, and those with a ratio higher than or equal to one can be formed by one-time photolithography. Chips with the ratio of width to height less than 1 were made by overlaying photolithography, which could increase the height by 200 μm each time. After that, mixed PDMS (20:1) was used to cast on the silicon wafer and baked at 80 ℃ for 2h. The sealing layer was prepared similarly and was bonded with the fluidics layer after oxygen plasma treatment. Afterward, one end of the chip was fixed on the slide platform, and the other end was fixed on the bracket by double-sided tape (9448A, 3M, America) and adhesive tape (810-HH10, 3M, America). 20 μl blue dye was added to the entrance of the chip. Next, the stepper motor was driven to a specific location on the PC side to obtain different deformation. During the

process, a cellphone camera (HuaweiP30, android operating system, Shenzhen, China) was used to capture the image, illustrating the change of liquid.

2.8 DNA amplification in tubes and chips

Each positive 18 μl LAMP reaction consisted of 7.2 μl colorimetric LAMP 2X master mix, 8 μl nuclease-free H_2O, 1.8 μl N1 segment primers (Table 2), and 1 μl 2019-nCoV-N DNA plasmid. In contrast, negative controls contained 1 μl nuclease-free H_2O instead of 2019-nCoV-N DNA plasmid. All reagents were added to the tube for tube reactions, and then the tube was put in a metal bath at 65 ℃ for 40 min after mixing well. Firstly, to observe chip reactions, well-mixed (7.2 μl colorimetric LAMP 2X master mix and 1.8 μl N1 segment primers) reaction solution was pre-stored in the butterfly-shaped pipe of the chip. Subsequently, positive controls contained 1 μl 2019-nCoV-N DNA plasmid, and 8 μl nuclease-free H_2O was inhaled into the flow channel by capillary force. Negative controls replaced DNA plasmid with nuclease-free H_2O. After that, the chip was stretched so that the reaction solution and sample solution were mixed into the detection chamber. Finally, the chip was set on a metal heating plate for 40 min, whose temperature was set to 70 ℃ to ensure that the temperature inside the flexible chip was around 65 °C.

2.9 Statistical analyses

The Microsoft Excel and Origin 2018 software were used for the statistical analysis including Two-sample t test. Significant differences were indicated as * ($p \leq 0.05$), ** ($p \leq 0.01$), or *** ($p \leq 0.001$) according to the level of significance. The three-channel extraction of the image color in the article was processed by Matlab software, which calculated the mean value of the pigment points in the selected area.

3. Results

3.1 Principle of the stretchable chip for nucleic acid detection

The chip consisted of three layers (Fig, 1a), and the primary structure was integrated into the flow channel layer; the cover layer was used to seal the flow channel layer and connect the inlet and outlet with the atmosphere; the sealing layer not only played the role of sealing the detection chamber but also deepened the detection chamber by 0.7 mm. In order to reduce the influence of chip thickness on its stretching effect, the sealing layer was made shorter than the flow channel layer. The physical picture of the device was shown in Fig. 1b, which was thin and soft. The structure of the fluidics layer was shown in detail in Fig. 1c, and the reaction solution was pre-stored in the right flow channel. When the device was needed, the sample solution entered the microchannel from the inlet by capillary action Then, the strain valve burst (Fig. 1d) and generated a negative pressure because the chip was deformed. At that time, the sample solution and reaction solution were mixed through the spring pump flow channel. Finally, it arrived at the detection chamber for nucleic acid amplification at 65 ℃ for 40 min. During the nucleic acid amplification process, hydrogen ions would be released, which would cause a pH drop of the solution, and the pH indicator in the reaction solution can produce a color change visible to the naked eye. In this reaction system, if the solution remains pink, the sample is negative, and if it turns yellow, the sample is positive. The PH indicator is pink between 8.2 and 8.6 and turns yellow when the pH drops.

3.2 Material selection and modification

The mechanical properties of PDMS are related to the ratio of curing agents. Therefore, adjusting the ratio of curing agents can optimize the performance of the material. During the

use of the microfluidic chip, the material was required to have a certain degree of elasticity, which could achieve deformation. In order to select the most suitable ratio, the elastic modulus of the four PDMS with curing agent ratios of 10:1, 15:1, 20:1, and 25:1 were measured, and the stress-strain curves of the four groups were shown in Fig. 2a, in which the slope of the curve represented the modulus of elasticity. The elastic modulus of four groups of PDMS specimens was measured multiple times to obtain the results in Fig. 2b. The elastic modulus of the ratio 10:1 was 2.17 MPa, and the elastic modulus of the ratio 15：1 was 1.12 MPa. When the ratio was increased to 20:1, the elastic modulus was 0.52MPa, and the elastic modulus was 0.35MPa when the ratio was increased to 25:1. It can be seen that the relationship between the ratio of elastic modulus and curing agent was logarithmic instead of linear, which indicated that as the curing agent decreased, the elastic modulus of the PDMS specimen would decrease. The better its tensile properties, the easier it was for users to use. However, when the amount of the curing agent was too little, it was not easy for PDMS to form. In the experiment, when the ratio was 25:1, the surface of the specimen after forming was relatively sticky. Considering the elastic modulus and molding effect, the ratio of curing agent used in the experiment should be 20:1.

PDMS was a hydrophobic material, and its contact angle measurement was shown in Fig. 2f. A capillary force was required to suck the sample into the liquid storage channel in this device, so the liquid storage channel needed to be modified to be hydrophilic. There were a large number of methods for surface modification of PDMS, such as plasma cleaning and ultraviolet light irradiation, but their timeliness was poor. In order to compare the timeliness of different treatment methods, five groups of smooth PDMS surface, PVP(polyvinyl pyrrolidone) solution coating surface, plasma treatment surface, PVP solution coating surface after plasma treatment,

and plasma treatment surface after PVP solution coating were designed. First, the five sets of initial contact angles were measured. The results were shown in Fig. 2c. The surface contact angle after PVP solution coating was 66° (Fig. 2h), and the surface contact angle after plasma treatment was 23° (Fig. 2g). The surface contact after plasma treatment after PVP solution coating The angle was 16°, and the contact angle of the PVP solution coated surface after plasma treatment was 34° (Fig. 2i). It was found that the hydrophilic surface effect after plasma treatment was the best comparing the five groups, and the effect of PVP solution coating treatment was inadequate. Six days later, the contact angles of the five groups were measured, as shown in Fig. 2d. The contact angles of the first four groups were all around 90°, but the contact angle of the fifth group was 37°. Namely, the hydrophilicity was still effective.

In conclusion, coating the surface with PVP solution after plasma treatment could effectively make the surface of PDMS hydrophilic and had a specific aging property. In addition, the contact angle of different body fluids on the hydrophilic modified surface was measured (Fig. 2e) to prove the universality of the hydrophilic modification method. The contact angle of culture medium was 25°, sweat 42°, saliva 32°, blood 18°, and ethanol 10°.

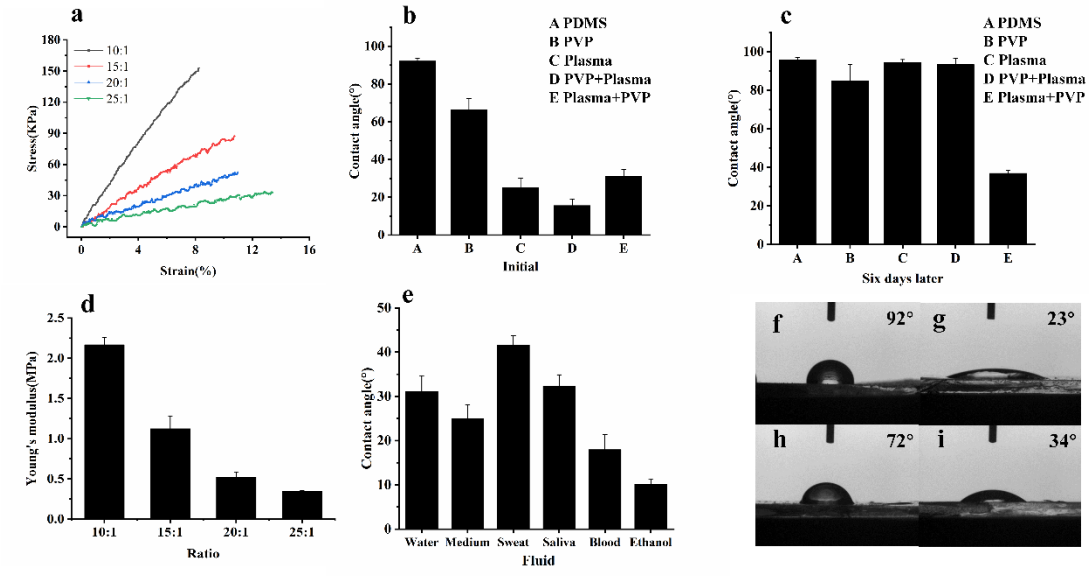

Fig 2 PDMS material performance measurement. **a** PDMS stress-strain curves of different proportions of curing agent. **b** Initial contact angle after different treatments. **c** Contact angle after different treatments after six days. **d** PDMS Young's modulus of different curing agent ratios. **e** Contact angle of PDMS surface after treatment of different solutions. **f** Contact angle of PDMS surface without surface treatment. g Plasma treatment PDMS surface contact angle. **h** PDMS contact angle after PVP solution coating treatment. **i** The contact angle of the PVP solution coated surface after plasma treatment.

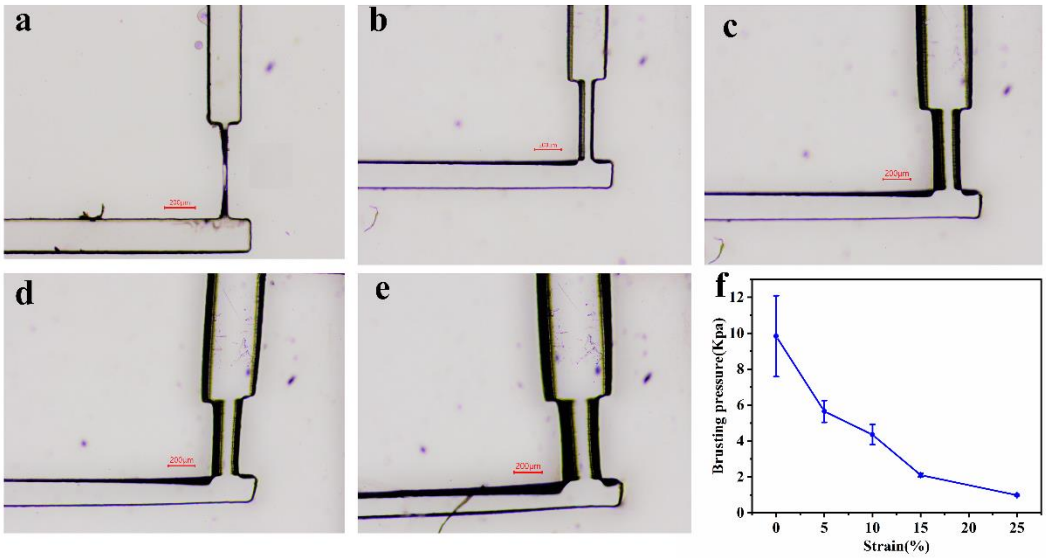

Fig 3 Strain valve deformation diagram. **a** No deformation of strain valve shape. **b** 5% deformation strain valve form. **c** 10% deformation strain valve form. **d** 15% deformation strain valve form. **e** 25% deformation strain valve form. **f**. Curves of burst pressure of strain valve under different deformations.

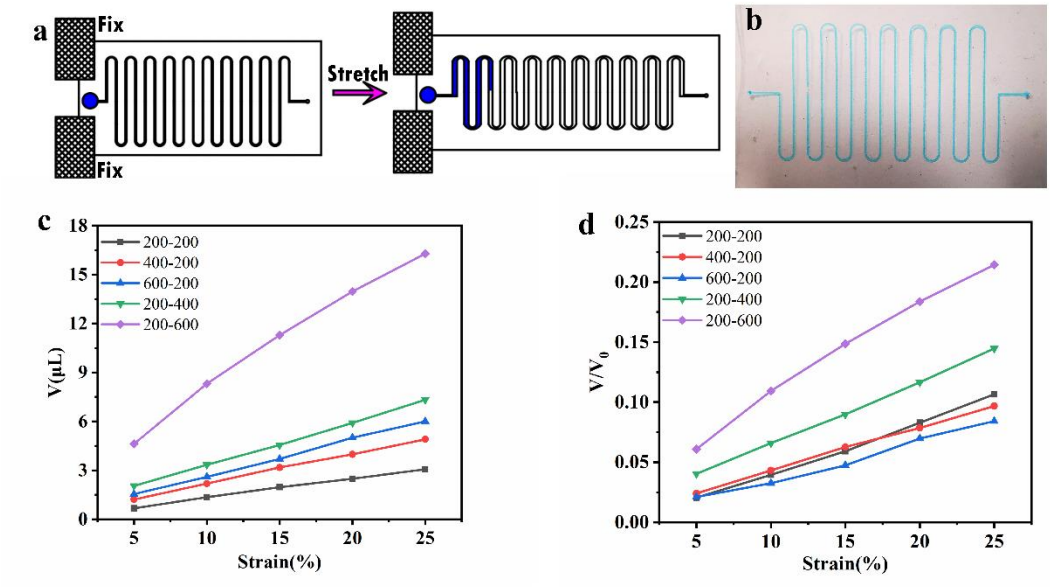

Fig 4 Optimized aspect ratio of the spring pump. **a** Schematic diagram of spring pump. **b** Physical picture

of spring pump. **c** The relationship curve between volume extraction and deformation of spring pumps with different aspect ratios. **d** The relationship curve between volume extraction volume, total volume ratio, and deformation of spring pumps with different aspect ratios.

3.3 Soft strain valve

The structure of the stain valve was shown in Fig. 1d in detail, composed of a structure with a high aspect ratio (height (200 μm): width (25 μm)). In the absence of deformation, due to the presence of van der Waals force, the PDMS on both sides were bonded together and customarily closed (Fig. 3a), which could prevent the pre-existing reaction solution from flowing down. In the case of deformation, the area increased, and the valve opened. During this process, the van der Waals force was reversible and temporary, so the valve can be restored to the initial state after the release of deformation, which ensured the repeatability of the valve so that the chip could be stretched multiple times. As the deformation degree increased, the area of the strain valve also became larger in Fig. 3b-3e. If users couldn't provide a large force drive, they could only rely on the tensile force of their hands to drive. Therefore, it was necessary to measure the burst pressure of the strain valve of the equipment. As shown in Fig. 3f, as the deformation amount increased, the burst pressure gradually decreased. When the deformation amount equaled 0, the burst pressure was 10Kpa, and when the deformation amount equaled 20%, the burst pressure was close to 2Kpa, which was easy to breakthrough.

3.4 Microfluidic spring pump

The working principle of the spring pump was as follows. The serpentine flow channel on the device was deformed by stretching (Fig. 4a), which caused the volume in the fluidic channel to change, generating a negative pressure. The fluid was driven to flow in a specific direction. The volume change was related to the size of the deformation and the size of the pump. In order to

optimize the size of the pump, five sets of pumps with aspect ratios of 0.33, 0.5, 1.0, 2.0, and 3.0 were designed. The actual picture of the experiment was shown in Fig. 4b. The experimental results showed that under the same deformation, the height had a more significant influence on the volume change than the width of the spring pump. A pump with a cross-sectional area of 200 μm * 600 μm produced a volume change of 16.2 μl when the deformation was 25% in Fig. 4c. When the height of the pump was 200 μm, the width increased from 200 μm to 400 μm and 600 μm, and the volume increased produced by the same deformation amount didn't exceed 3 μl at most. When the width of the pump was 200 μm, the height increased from 200 μm to 400 μm and 600 μm, and the volume caused by the same deformation increased exponentially. The volume normalization parameters were shown in Fig. 4d, and it could be seen more clearly that the height had a more significant influence. Comparing the three sets of curves with ratios of 0.33, 1.0, and 3.0, it was found that the greater the ratio, the greater the slope of the curve, which also meant that the higher the ratio, the greater the influence of the deformation on the volume change rate.

3.5 Chip performance test

After parameter optimization, different color dyes were used to test the performance of the chip. Firstly, the red and blue dyes were sucked in by capillary force, then, stretching the lower end of the chip, the dye broke through the strain valve and entered the serpentine spring flow channel. Repeated stretching allowed the two dyes to mix well and flow into the assay chamber, where the dye could be seen to change to purple. As the number of stretches increased, the amount of dye in the detection chamber increased and gradually filled the chamber (Fig 5).

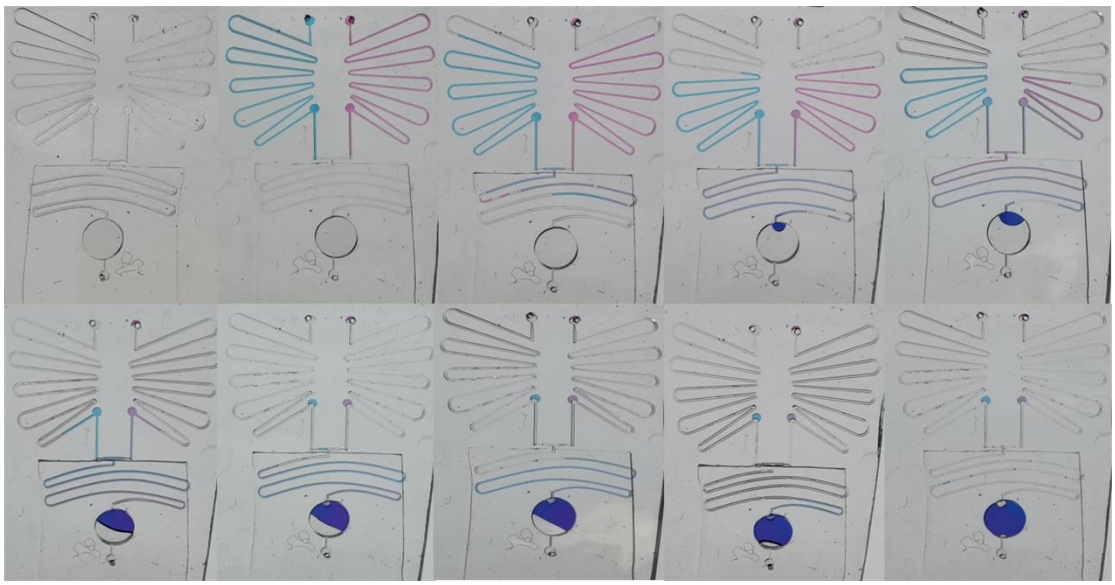

Fig 5 Physical image of fluid flow. The blue ink represented the reaction solution and the red ink represented the sample. By stretching, the two solutions gradually mixed and flowed into the assay chamber.

3.6 DNA amplification colorimetric reaction

For a more concise observation of the test results, the endpoint assay was performed using the LAMP colorimetric method. The initial color of the reaction solution and sample solution after mixing was pink. After the LAMP reaction, if the solution turned yellow, it meant that the sample was positive. Otherwise, the sample was negative if the solution remained pink, as shown in Fig.6a. The RGB of the positive result extracted from the test tube was shown in Fig. 6c, the maximum errors of which for different reaction chambers were 5.3%, 9.4%, and 2.5%, indicating a good consistency. The RGB result of the negative extracted from the test tube was shown in Fig. 6f, the maximum errors of which for different reaction chambers were 7.3%, 4.5%, and 13.8%, indicating a good consistency. For the chip, determining whether the initial sample was negative or positive by judging the color of the endpoint was the same as for the test tube (Fig. 6b). The RGB images obtained by repeating the nucleic acid amplification experiments on the chip were shown in Fig. 6d (positive) and Fig. 6g (negative). It could be seen that a significant difference between the positive and negative results was the G value. To

further quantify the difference between negative and positive results, the normalized value (K=G/(R+G+B)) was set as a criterion to distinguish between negative and positive results. As shown in Fig. 6e, the K values of positive and negative reaction chambers were significantly different (p value ≤ 0.001) whether in chips or tubes.

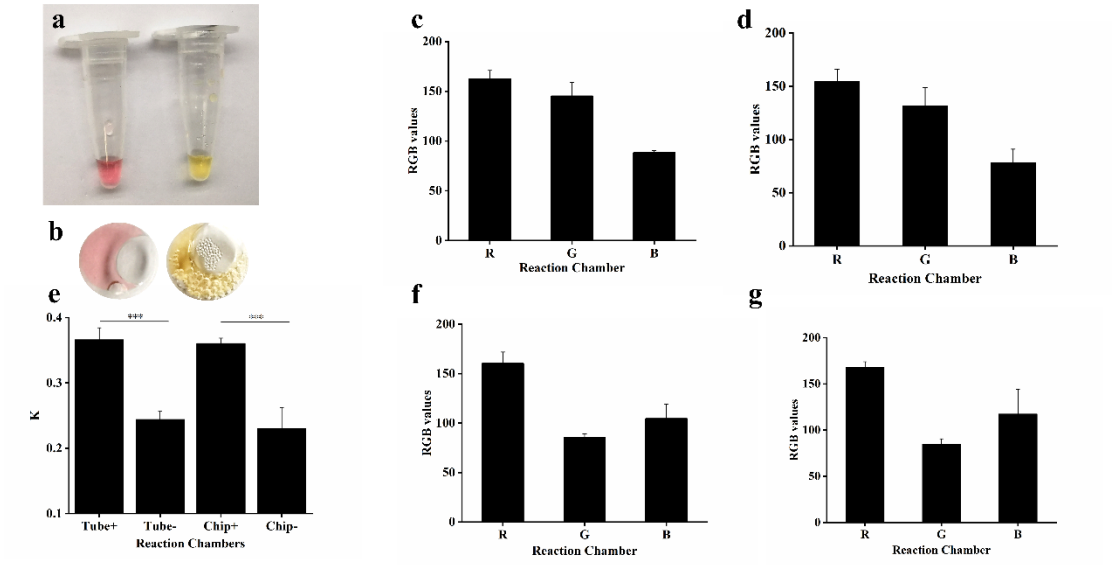

Fig 6 Nucleic acid amplification results. **a** Negative and positive results of nucleic acid amplification in the test tube. **b** Negative and positive results of nucleic acid amplification on the chip. **c** RGB analysis chart of the positive result in the test tube. **d** RGB analysis chart of the positive result on the chip. **e** Comparison of K value of negative and positive results in the test tube and the chip. **f** RGB analysis chart of the negative result in the test tube. **g** RGB analysis chart of the negative result on the chip.

4. Discussion

This paper developed a flexible and straightforward microfluidic device whose detection results could be directly observed by the naked eye without relying on external electronic devices or active components. The color of the solution could determine positive and negative results. The hand-made microfluidic chip was less costly and had the potential for application in POCT diagnostics. The core design of the chip was a strain valve and a spring-loaded pump whose deformation generated a driving force similar to that of a spring. LOC devices' different techniques to achieve passively driven were surface

tension, vacuum suction, and pressure-driven (Narayanamurthy et al., 2020). Stretch-driven was a new type of passively driven. The advantage of surface tension driven was that the fluid could be self-driven by surface chemical gradients or roughness. However, it was limited by the surface tension coefficient of the fluid(Zhu & Wang, 2016). The advantage of vacuum suction was versatile and portable, but the method was limited by the size of the vacuum chamber and was not repeatable(Hamon et al., 2016). Stretch-driven could provide a driving force that correlated well with the size of the deformation and was reusable. The finger-pressure microfluidic pump (Lu et al., 2020; Park & Park, 2019) was one kind of pressure-driven. The pump's performance depended on the microfluidic chip processing process, which required a certain airtightness between the air channel layer and the flow channel layer. Otherwise, air and liquid leakage was easy to occur. The chip designed in this paper contained only the flow channel layer, which didn’t require high confinement for processing and reduced the complexity of the chip manufacturing process. However, the finger-pressure microfluidic pump could achieve quantitative pumping of fluid(Park, Roh, & Park, 2019), while the stretch-type chip couldn’t achieve quantitative pumping.

In the article, by extracting the RGB values of the solution before and after the reaction, and comparing them, it was found that the chip could achieve the same detection effect as that of the test tube. In addition, the chip has the following advantages compared with the test tube. First, the chip relied only on the capillary force to take samples, which saved the standard laboratory consumables and reduced common support instruments. Second, the relatively shallow flow path of the chip made it more suitable for

microscopic samples collected from the surface of the human body, such as sweat, tears, and urine. The chip material used in our experiments was PDMS, which had the disadvantage of being hydrophobic and reverting to hydrophobicity relatively quickly after hydrophilic treatment(Gokaltun, Yarmush, Asatekin, & Usta, 2017). In this paper, we used plasma treatment followed by coating with PVP solution to extend the hydrophilic modification of the material. The contact angle of the modified surface was still less than 90° after six days later. In addition, the color can could be seen more visually on the chip. It is not easy to observe the color change in real-time when the test tube is in a metal bath, and if the test tube is heated on a heating plate, there is a problem of uneven heating.

Furthermore, the chip also has some areas for improvement. First, the nucleic acid amplification method used in this paper was LAMP with a holding temperature of 65°C. Considering the use of RPA amplification method, the required temperature is 37°C, which can be achieved by body temperature and made into a wearable device. Second, some microstructures can be added to the flow channel of the spring pump to achieve the effect of interfering with the laminar flow, which can enhance the fluid mixing effect. Third, the chip material can be considered to use other flexible new materials to reduce the cost and better apply to production. More importantly, the chip can be surface modified, embedded with resin beads or embedded with reaction paper (Pang et al., 2018) to adsorb impurities and achieve extraction and purification of DNA or RNA before amplification. In future work, we plan to integrate purifying samples into the chip (Chen et al., 2021).

In summary, a nucleic acid detection tool that does not require the cooperation of external equipment or expert-assisted judgment is of great practical value. This device has the potential of POCT, especially in remote areas where medical resources are scarce. In addition, it can be extended to home diagnostics to achieve personalized test feedback.

5. Conclusion

This paper proposed a stretched microfluidic chip for nucleic acid detection. According to the mechanical properties of the material, a suitable ratio of PDMS to curing agent was selected to be 20:1, and a hydrophilic modification method was proposed in which the PDMS surface was cleaned by plasma and then coated with PVP solution, which verified that its timeliness was better. In addition, the performance analysis of the strain valve structure of the chip and the burst pressure measurement proved its feasibility. The aspect ratio of the spring pump was optimized, and it was found that the height had a more significant influence on the pump's performance. Nucleic acid testing of COVID-19 was performed on the chip and test tube, and it was found that both the chip and the test tube could achieve the qualitative detection of negative and positive samples.

Acknowledgments

All data generated or analyzed in this study are included either in this article and/or in the supplementary information files.

Author contributions

Jiajun Huang and Shengli Mi conceived this study. Xiang Li designed and performed experiments. Shengli Mi, Jiajun Huang, Xiang Li wrote and revised the manuscript. Xiaoyu Zhao, Weihao Yang, Fei Xua, Bailiang Chen, Jiwei Peng, performed the experiments, analyzed

data, and commented on the manuscript.

Competing interests

The authors declare that this article's content has no known conflicts of interest.

Funding

This work was funded by the Project of Basic Research of Shenzhen, China (JCYJ20180507183655307 & JCYJ20190813143221901). SL Mi and JJ Huang received the funding. The funders had no role in study design, data collection and analysis, decision to publish, or preparation of the manuscript. There are no financial conflicts of interest to disclose.

Reference

Bandodkar, A. J., Jia, W., Yardimci, C., Wang, X., Ramirez, J., & Wang, J. (2015). Tattoo-Based Noninvasive Glucose Monitoring: A Proof-of-Concept Study. *Anal Chem, 87*(1), 394-398. doi:10.1021/ac504300n

Chen, P., Chen, C., Su, H., Zhou, M., Li, S., Du, W., . . . Liu, B. F. (2021). Integrated and finger-actuated microfluidic chip for point-of-care testing of multiple pathogens. *Talanta, 224*, 121844. doi:10.1016/j.talanta.2020.121844

Compton, J. (1991). NUCLEIC-ACID SEQUENCE-BASED AMPLIFICATION. *Nature, 350*(6313), 91-92. doi:10.1038/350091a0

Gokaltun, A., Yarmush, M. L., Asatekin, A., & Usta, O. B. (2017). Recent advances in nonbiofouling PDMS surface modification strategies applicable to microfluidic technology. *Technology (Singap World Sci), 5*(1), 1-12. doi:10.1142/S2339547817300013

Gong, S., Schwalb, W., Wang, Y., Chen, Y., Tang, Y., Si, J., . . . Cheng, W. (2014). A wearable and highly sensitive pressure sensor with ultrathin gold nanowires. *Nat Commun, 5*, 3132. doi:10.1038/ncomms4132

Hamon, C., Henriksen-Lacey, M., La Porta, A., Rosique, M., Langer, J., Scarabelli, L., . . . Basabe-Desmonts, L. (2016). Tunable Nanoparticle and Cell Assembly Using Combined Self-Powered Microfluidics and Microcontact Printing. *Advanced Functional Materials, 26*(44), 8053-8061. doi:10.1002/adfm.201602225

Ji, M., Xia, Y., Loo, J. F.-C., Li, L., Ho, H.-P., He, J., & Gu, D. (2020). Automated multiplex nucleic acid tests for rapid detection of SARS-CoV-2, influenza A and B infection with direct reverse-transcription quantitative PCR (dirRT-qPCR) assay in a centrifugal microfluidic platform. *RSC Advances, 10*(56), 34088-34098. doi:10.1039/d0ra04507a

Kang, Y. J. (2019). Simultaneous measurement of blood pressure and RBC aggregation by monitoring on-off blood flows supplied from a disposable air-compressed pump. *Analyst, 144*(11), 3556-3566. doi:10.1039/c9an00025a

Koh, A., Kang, D., Xue, Y., Lee, S., Pielak, R. M., Kim, J., . . . Rogers, J. A. (2016). A soft, wearable

microfluidic device for the capture, storage, and colorimetric sensing of sweat. *Science Translational Medicine, 8*(366), 13. doi:10.1126/scitranslmed.aaf2593

Koonin, L. M. (2020). Novel coronavirus disease (COVID-19) outbreak: Now is the time to refresh pandemic plans. *Journal of business continuity & emergency planning, 13*(4), 1-15.

Lee, H., Park, W., Ryu, H., & Jeon, N. L. (2014). A microfluidic platform for quantitative analysis of cancer angiogenesis and intravasation. *Biomicrofluidics, 8*(5), 054102. doi:10.1063/1.4894595

Lee, H. B., Meeseepong, M., Trung, T. Q., Kim, B. Y., & Lee, N. E. (2020). A wearable lab-on-a-patch platform with stretchable nanostructured biosensor for non-invasive immunodetection of biomarker in sweat. *Biosens Bioelectron, 156*, 112133. doi:10.1016/j.bios.2020.112133

Li, B., Qiu, Y., Glidle, A., McIlvenna, D., Luo, Q., Cooper, J., . . . Yin, H. (2014). Gradient microfluidics enables rapid bacterial growth inhibition testing. *Anal Chem, 86*(6), 3131-3137. doi:10.1021/ac5001306

Liu, D., Zhu, Y., Li, N., Lu, Y., Cheng, J., & Xu, Y. (2020). A portable microfluidic analyzer for integrated bacterial detection using visible loop-mediated amplification. *Sensors and Actuators B: Chemical, 310*, 127834. doi:10.1016/j.snb.2020.127834

Lu, C. H., Shih, T. S., Shih, P. C., Pendharkar, G. P., Liu, C. E., Chen, C. K., . . . Liu, C. H. (2020). Finger-powered agglutination lab chip with CMOS image sensing for rapid point-of-care diagnosis applications. *Lab Chip, 20*(2), 424-433. doi:10.1039/c9lc00961b

Mori, Y., Kitao, M., Tomita, N., & Notomi, T. (2004). Real-time turbidimetry of LAMP reaction for quantifying template DNA. *J Biochem Biophys Methods, 59*(2), 145-157. doi:10.1016/j.jbbm.2003.12.005

Mori, Y., Nagamine, K., Tomita, N., & Notomi, T. (2001). Detection of loop-mediated isothermal amplification reaction by turbidity derived from magnesium pyrophosphate formation. *Biochemical and Biophysical Research Communications, 289*(1), 150-154. doi:10.1006/bbrc.2001.5921

Narayanamurthy, V., Jeroish, Z. E., Bhuvaneshwari, K. S., Bayat, P., Premkumar, R., Samsuri, F., & Yusoff, M. M. (2020). Advances in passively driven microfluidics and lab-on-chip devices: a comprehensive literature review and patent analysis. *RSC Advances, 10*(20), 11652-11680. doi:10.1039/d0ra00263a

Nguyen, H. V., Nguyen, V. D., Nguyen, H. Q., Chau, T. H. T., Lee, E. Y., & Seo, T. S. (2019). Nucleic acid diagnostics on the total integrated lab-on-a-disc for point-of-care testing. *Biosens Bioelectron, 141*, 111466. doi:10.1016/j.bios.2019.111466

Notomi, T., Okayama, H., Masubuchi, H., Yonekawa, T., Watanabe, K., Amino, N., & Hase, T. (2000). Loop-mediated isothermal amplification of DNA. *Nucleic Acids Research, 28*(12), 7. doi:10.1093/nar/28.12.e63

Oh, S. J., & Seo, T. S. (2019). Combination of a centrifugal microfluidic device with a solution-loading cartridge for fully automatic molecular diagnostics. *Analyst, 144*(19), 5766-5774. doi:10.1039/c9an00900k

Pang, B., Fu, K., Liu, Y., Ding, X., Hu, J., Wu, W., . . . Li, J. (2018). Development of a self-priming PDMS/paper hybrid microfluidic chip using mixed-dye-loaded loop-mediated isothermal amplification assay for multiplex foodborne pathogens detection. *Anal Chim Acta, 1040*, 81-89. doi:10.1016/j.aca.2018.07.024

Park, J., & Park, J. K. (2019). Integrated microfluidic pumps and valves operated by finger actuation. *Lab Chip, 19*(18), 2973-2977. doi:10.1039/c9lc00422j

Park, J., Roh, H., & Park, J. K. (2019). Finger-Actuated Microfluidic Concentration Gradient Generator Compatible with a Microplate. *Micromachines (Basel), 10*(3). doi:10.3390/mi10030174

Reeder, J. T., Xue, Y., Franklin, D., Deng, Y., Choi, J., Prado, O., . . . Rogers, J. A. (2019). Resettable skin interfaced microfluidic sweat collection devices with chemesthetic hydration feedback. *Nat Commun, 10*(1), 5513. doi:10.1038/s41467-019-13431-8

Schuler, F., Schwemmer, F., Trotter, M., Wadle, S., Zengerle, R., von Stetten, F., & Paust, N. (2015). Centrifugal step emulsification applied for absolute quantification of nucleic acids by digital droplet RPA. *Lab Chip, 15*(13), 2759-2766. doi:10.1039/c5lc00291e

Sempionatto, J. R., Brazaca, L. C., Garcia-Carmona, L., Bolat, G., Campbell, A. S., Martin, A., . . . Wang, J. (2019). Eyeglasses-based tear biosensing system: Non-invasive detection of alcohol, vitamins and glucose. *Biosens Bioelectron, 137*, 161-170. doi:10.1016/j.bios.2019.04.058

Song, Q., Sun, X., Dai, Z., Gao, Y., Gong, X., Zhou, B., . . . Wen, W. (2021). Point-of-care testing detection methods for COVID-19. *Lab Chip*. doi:10.1039/d0lc01156h

Strohmeier, O., Marquart, N., Mark, D., Roth, G., Zengerle, R., & von Stetten, F. (2014). Real-time PCR based detection of a panel of food-borne pathogens on a centrifugal microfluidic "LabDisk" with on-disk quality controls and standards for quantification. *Analytical Methods, 6*(7). doi:10.1039/c3ay41822g

Syedmoradi, L., Norton, M. L., & Omidfar, K. (2021). Point-of-care cancer diagnostic devices: From academic research to clinical translation. *Talanta, 225*, 122002. doi:10.1016/j.talanta.2020.122002

Tanner, N. A., Zhang, Y., & Evans, T. C., Jr. (2015). Visual detection of isothermal nucleic acid amplification using pH-sensitive dyes. *Biotechniques, 58*(2), 59-68. doi:10.2144/000114253

Temmerman, R., Huys, G., & Swings, J. (2004). Identification of lactic acid bacteria: culture-dependent and culture-independent methods. *Trends in Food Science & Technology, 15*(7-8), 348-359. doi:10.1016/j.tifs.2003.12.007

Vincent, M., Xu, Y., & Kong, H. M. (2004). Helicase-dependent isothermal DNA amplification. *Embo Reports, 5*(8), 795-800. doi:10.1038/sj.embor.7400200

Yang, B., Fan, Y., Li, Y., Yan, J., Fang, X., & Kong, J. (2020). Rapid and simultaneous analysis of twelve virulence factor genes by a microfluidic-CFPA chip for identifying diarrheagenic Escherichia coli. *Analyst, 145*(11), 3814-3821. doi:10.1039/c9an02572c

Yang, X., Yao, H., Zhao, G., Ameer, G. A., Sun, W., Yang, J., & Mi, S. (2020). Flexible, wearable microfluidic contact lens with capillary networks for tear diagnostics. *Journal of Materials Science*. doi:10.1007/s10853-020-04688-2

Ye, X., Li, Y., Wang, L., Fang, X., & Kong, J. (2021). All-in-one microfluidic nucleic acid diagnosis system for multiplex detection of sexually transmitted pathogens directly from genitourinary secretions. *Talanta, 221*, 121462. doi:10.1016/j.talanta.2020.121462

Yu, N., Liu, Y., Ji, B., Wang, S., Chen, Y., Sun, T., . . . Yang, B. (2020). High-sensitivity microliter blood pressure sensors based on patterned micro-nanostructure arrays. *Lab Chip, 20*(9), 1554-1561. doi:10.1039/d0lc00063a

Yu, Z., Lyu, W., Yu, M., Wang, Q., Qu, H., Ismagilov, R. F., . . . Shen, F. (2020). Self-partitioning SlipChip for slip-induced droplet formation and human papillomavirus viral load quantification with digital LAMP. *Biosens Bioelectron, 155*, 112107. doi:10.1016/j.bios.2020.112107

Zhang, F., Ma, L., Xu, Z., Zheng, J., Shi, Y., Lu, Y., & Miao, Y. (2009). Sensitive and rapid detection of Karenia mikimotoi (Dinophyceae) by loop-mediated isothermal amplification. *Harmful Algae,*

8(6), 839-842. doi:10.1016/j.hal.2009.03.004

Zhang, Y., Chen, Y., Huang, J., Liu, Y., Peng, J., Chen, S., . . . Wang, X. (2020). Skin-interfaced microfluidic devices with one-opening chambers and hydrophobic valves for sweat collection and analysis. *Lab Chip, 20*(15), 2635-2645. doi:10.1039/d0lc00400f

Zhang, Z., Azizi, M., Lee, M., Davidowsky, P., Lawrence, P., & Abbaspourrad, A. (2019). A versatile, cost-effective, and flexible wearable biosensor for in situ and ex situ sweat analysis, and personalized nutrition assessment. *Lab Chip, 19*(20), 3448-3460. doi:10.1039/c9lc00734b

Zhang, Z., Pi, Z., & Liu, B. (2015). TROIKA: a general framework for heart rate monitoring using wrist-type photoplethysmographic signals during intensive physical exercise. *IEEE Trans Biomed Eng, 62*(2), 522-531. doi:10.1109/TBME.2014.2359372

Zhu, P., & Wang, L. (2016). Passive and active droplet generation with microfluidics: a review. *Lab Chip, 17*(1), 34-75. doi:10.1039/c6lc01018k